

## DIRAC DISPERSION AND ZERO-INDEX IN TWO DIMENSIONAL AND THREE DIMENSIONAL PHOTONIC AND PHONONIC SYSTEMS (INVITED PAPER)

C. T. Chan\*, X. Huang, F. Liu, and Z. H. Hang

Department of Physics, Hong Kong University of Science and Technology, Clear Water Bay, Kowloon, Hong Kong, China

**Abstract**—We show that by applying accidental degeneracy, we can obtain a triply-degenerate state at the zone center in the band diagram of two dimensional (2D) photonic crystal. The dispersion near the zone center comprises two linear bands and an additional flat band crossing at the same frequency. If this triply-degenerate state is formed by the degeneracy of monopole and dipole excitations, we show that the system can be mapped to an effective medium with permittivity and permeability equal to zero. While “Dirac cone” dispersions can only be meaningfully defined in 2D systems, the notion of a Dirac point can be extended to three dimensional (3D) classical wave systems. We show that a simple cubic photonic crystal composed of core-shell spheres exhibits a 3D Dirac-like point at the center of the Brillouin zone at a finite frequency. Using effective medium theory, we can map our structure to an isotropic zero refractive index material in which the effective permittivity and permeability are simultaneously zero at the Dirac-like point frequency ( $\omega_D$ ). The Dirac-like point is six-fold degenerate and is formed by the accidental degeneracy of electric dipole and magnetic dipole excitations, each with three degrees of freedom. We found that 3D Dirac-like points at  $\vec{k} = 0$  can also be found in simple cubic acoustic wave crystals. Different from the case in the photonic system, the 3D Dirac-like point in acoustic wave system is four-fold degenerate, and is formed by the accidental degeneracy of dipole and monopole excitations. Using effective medium theory, this acoustic wave system can also be described as a material which has both effective mass density and reciprocal of bulk modulus equal to zero at  $\omega_D$ . For both the photonic and phononic systems, a subset of the bands has linear dispersions near the zone center, and they give

---

*Received 21 August 2012, Accepted 17 September 2012, Scheduled 20 September 2012*

\* Corresponding author: Che-Ting Chan (phchan@ust.hk).

rise to equi-frequency surfaces that are spheres with radii proportional to  $(\omega - \omega_D)$ .

## 1. INTRODUCTION

Natural materials owe their optical properties to the properties of the individual atoms/molecules as well as the lattice structure which dictates how the atoms/molecules are arranged. As the optical wavelength is typically a thousand times longer than the atomic lattice constant, we can average the light propagation properties over the atomic scale and describe the interaction between light and materials by macroscopic electromagnetic parameters: the permittivity and permeability. The permittivity can be either positive or negative, while at higher frequencies, the relative permeability is almost equal to 1 [1]. In 1968, Veselago proposed the concept of materials with negative permittivity and permeability simultaneously [2] and various intriguing electromagnetic wave propagation properties were predicted. However, such materials do not exist in nature. It is only until 1999 that Pendry et al. proposed to use resonating conducting elements to realize negative permeability [3], and the concept was soon realized experimentally in a material with both negative effective permittivity ( $\varepsilon_{eff}$ ) and effective permeability ( $\mu_{eff}$ ) [4], and negative refraction was successfully demonstrated as predicted. We now call these composite materials “metamaterials”, and various types of metamaterials with all kinds of effective permittivity ( $\varepsilon_{eff}$ ) and effective permeability ( $\mu_{eff}$ ) were designed and novel physical phenomena have been realized, including negative refraction [4–8], imaging [9–14], cloaking [15–21], illusion [22] and reversed Cherekov Radiation [23]. In short, by realizing metamaterials with different effective permittivity and permeability, peculiar wave guiding properties can be achieved and the exploration of the parameter space of  $\varepsilon_{eff}$  and  $\mu_{eff}$  is extending mankind’s ability to control light and waves.

The two  $\varepsilon_{eff}$  and  $\mu_{eff}$  axes in the parameter space are particular, where the refractive index is equal to zero. In a homogeneous isotropic material, a zero-refractive-index material can be either single-zero ( $\varepsilon_{eff} = 0$  or  $\mu_{eff} = 0$ ) or double-zero ( $\varepsilon_{eff} = \mu_{eff} = 0$ ) [24–39]. The phase velocity of light in a zero-index material is much greater than the speed of light and can even approach infinity. As a consequence, the phase of light throughout a piece of zero-index material is essentially a constant, independent of its shape. This unique property leads to many intriguing phenomena and plausible applications, such as tailoring the radiation phase pattern of arbitrary sources [33–35], making wave guiding channels of arbitrarily shapes [24–32], and

cloaking objects in waveguides [36–39]. However, it is very difficult to realize zero-index materials in natural materials, let alone having it at any frequency we want. Recently, the rapid development of metamaterial has enabled the creation of single-zero-index materials by using complex subwavelength resonant structures [30]. Nevertheless, the design and fabrication procedures are complicated and absorption is inevitable in the single-zero-index metamaterials, which typically involve subwavelength metallic inclusions, and this would severely limit its functionality at optical frequencies. Moreover, the group velocity in a single-zero-index material is zero because it utilizes the band edge of a band gap, and the impedance of a single-zero-index material is either infinity or zero [35, 39]. These disadvantages can be avoided by using double-zero-index materials which possess finite group velocity and impedance.

It is straightforward to show that a dispersive homogenous system with  $\varepsilon = \mu = 0$  has linear dispersions (Dirac cone) at a particular frequency at  $\vec{k} = 0$ , and the linear dispersions will generate Dirac cones [40]. Many interesting physical properties of graphene are consequences of the Dirac cone dispersion in its electronic band structure [41–48]. It turns out that some classical wave systems such as 2D photonic and phononic crystals also possess Dirac cone dispersions [49–62]. Special transport properties such as “Zitterbewegung” [61–63] and some interesting physical properties such as the existence of non-trivial Berry phases [53–58] that originate from the Dirac cone in electronic systems can also be observed in classical wave Dirac cone systems. Most of the Dirac points, including those in graphene [41–48] and two dimensional (2D) classical wave systems [52–62], are found at the Brillouin zone boundary. It was recently discovered that Dirac points can also be realized at the zone center of 2D photonic [49] and phononic [50–51, 58] crystals. The physical origins of these  $\vec{k} = 0$  Dirac-like cones are different from the usual zone boundary Dirac cones. Whereas the zone boundary Dirac cones are consequences of the lattice symmetry, the existence of Dirac points at  $\vec{k} = 0$  requires some sort of accidental degeneracy. Without additional degeneracy, the dispersion of a non-degenerate band at  $\vec{k} = 0$  is always parabolic due to time reversal symmetry and parabolic bands cannot generate Dirac cones. Zone center Dirac-like cones are also accompanied by an extra flat band of states [49–51, 58], which makes the physics different from that of zone boundary Dirac cones. For example, the Berry phase enclosing a zone center Dirac-like point is zero [58] while the Berry phase associated with the Dirac cone in graphene is  $\pi$  [41–48]. In our previous paper, we found that a subset of such photonic crystals behave as if they have effectively  $\varepsilon = 0$  and

$\mu = 0$  at the Dirac-like point frequency [49], and the analogy can be extended to acoustic [50] and elastic [51] waves. It is important to note that the mapping of a  $\vec{k} = 0$  Dirac cone system to a double-zero metamaterial is meaningful only if the accidental degeneracy originates from the dipole and monopole degrees of freedom.

The notion of a Dirac “cone” is inherently a 2D concept. Recently, Sakoda showed that it is possible to find three dimensional (3D) Dirac-like points at the Brillouin zone center of cubic electromagnetic systems with  $O_h$  symmetry [64]. A 3D Dirac-like point can be created by the accidental degeneracy of a non-degenerate  $A_{1g}$  mode, and a triply-degenerate  $T_{1u}$  mode in 3D photonic systems [64]. The concept of Dirac point is hence extended from 2D to 3D. To make our discussion more straightforward, we will limit ourselves to isotropic systems in the following. The equi-frequency surfaces corresponding to 2D Dirac cones are elements of a set of circles whose radii decrease linearly and approach zero both from above and below the Dirac point and the Dirac point is the frequency at which the equi-frequency circle has zero radius. To obtain a Dirac cone, the dispersion must be linear near the zone center which requires accidental degeneracy. When concept is extended from 2D to 3D, the equi-frequency trajectories change from circles in 2D to spheres in 3D. Near the “Dirac point” in 3D systems, the radii of equi-frequency spheres are linearly proportional to  $(\omega - \omega_D)$  where  $\omega_D$  is the Dirac point frequency, and the Dirac point is the frequency at which the equi-frequency sphere becomes a point. The necessary condition is again linear dispersions near the zone center which requires accidental degeneracy.

While Sakoda has already shown mathematically that it is possible to extend the Dirac point concept to 3D and has shown using group theoretic method that such 3D Dirac-like point can be obtained using a singly-degenerate  $A_{1g}$  mode and a triply-degenerate  $T_{1u}$  mode in a simple cubic system [64], there is still more work to do. Firstly, we will explore whether some of these 3D Dirac-like point systems can be mapped to a system with  $\varepsilon_{eff} = \mu_{eff} = 0$  at the Dirac-like point, as in the case of 2D systems [49]. In addition, we want to explore whether there are simple physical systems that can realize such system with accidental degeneracy. For realization in physical systems, we note that the  $A_{1g}$  mode correspond to the monopolar excitations. This poses a challenge in practice because monopoles are difficult to construct in 3D photonic systems. The lowest order excitations are typically dipoles. We will show that the accidental degeneracy of 3D dipoles and monopoles can be realized instead in acoustic wave systems, and thereby obtaining Dirac-like points in 3D for acoustic crystals. For electromagnetic waves in 3D, it is more challenging but we will show

that there is another route to obtain a Dirac-like point. Using group theoretic method and by giving a specific example, we will show that 3D Dirac-like points can be obtained if electric and magnetic dipole excitations can be arranged to be accidentally degenerate at  $\vec{k} = 0$ .

More specifically, we demonstrate that core-shell spheres arranged in a simple cubic lattice exhibit a 3D Dirac-like point at the  $\Gamma$  point. The Dirac-like point consists of six-fold-degenerate states, formed by the triply-degenerate  $T_{1u}$  and  $T_{1g}$  modes. The  $T_{1u}$  and  $T_{1g}$  modes correspond to magnetic and electric dipoles respectively. Four of the six-fold-degenerate states have linear dispersions near the Dirac-like point, while the other two are quadratic. This Dirac-like point is different from the scheme proposed in Ref. [64], which is a four-fold-degenerate state. For acoustic wave systems, we found that a simple cubic system composing of rubber spheres embedded in the water can give a 3D Dirac-like point at the  $\Gamma$  point in the band structure and the Dirac-like point is formed by a four-fold-degenerate state. This four-fold-degenerate state comprises a non-degenerate monopole  $A_{1g}$  mode and a triply-degenerate dipole  $T_{1u}$  mode, which falls into the class of 3D Dirac-like point proposed in Ref. [64]. For the 3D acoustic wave system, the tight-binding method shown in Ref. [64] can be applied directly to prove the existence of the Dirac-like point. The 3D Dirac-like point in photonic systems has six degrees of freedom, and as such, the proof of the existence of the Dirac-like point is more tedious and the details will be shown in the appendix. Using effective medium theory, we will show that the structures with 3D Dirac-like point in photonic and phononic systems can be described as isotropic zero-refractive-index materials at the Dirac-like point frequency, in the sense that all components of the effective permittivity and permeability are equal to zero in the photonic system, and the effective mass density and reciprocal of bulk modulus are equal to zero in the phononic system.

The paper is organized as following. In Section 2, we will introduce the Dirac-like point in 2D photonic crystal. There is a triple degenerate state at the  $\Gamma$  point in the band structure. This triple degenerate state can be described by the linear combination of monopole and dipoles. Applying the effective medium theory, we can map the 2D photonic crystal to a homogenous zero-refractive-index material with both permittivity and permeability equal to zero simultaneously. In Sections 3 and 4, we will extend the concept of 2D Dirac-like point to 3D both in photonic and phononic systems. In photonic system, the Dirac-like point relates to a six-fold degenerate state which corresponding to electric and magnetic dipoles, while in phononic system, it relates to a four-fold degenerate state which corresponding to monopole and dipoles. Both the 3D photonic and phononic crystals

with 3D Dirac-like point at the zone center can be described using the effective medium theory as a homogeneous material with permittivity and permeability equal to zero simultaneously in photonic system and with mass density and reciprocal of bulk modulus equal to zero simultaneously in phononic system. At last, we will give a summary.

## 2. 2D DIRAC-LIKE POINT IN PHOTONIC SYSTEM

Let us first consider a 2D photonic crystal that exhibits a Dirac-like point at the  $\Gamma$  point [49]. The band structure of a 2D photonic crystal consisting of a square lattice of dielectric cylinders for the transverse-magnetic (TM) polarization, with the electric field along the cylinder axis, is shown in Fig. 1(a) [49]. The radius and relative permittivity of the cylinders are set as  $R = 0.2a$  and  $\varepsilon_r = 12.5$ , where  $a$  is the lattice constant. There is a triply-degeneracy state at the  $\Gamma$  point, which comprises of two linear bands and another quadratic band intersecting at the same frequency. The quadratic band is nearly dispersionless near the zone center. We note that the triple degeneracy is “accidental”, meaning that it is not a consequence of lattice symmetry. If the systems parameters are changed (e.g., a different radius of the cylinder), the triple degenerate state will split into a doublet and a singlet. To visualize the Dirac-like cones, the dispersion surfaces are plotted in Fig. 1(c). There are clearly two touching cones at the  $\Gamma$  point (purple) and a flat sheet (green) crossing the Dirac-like point. In order to analyze the underlying physics of the triple degenerate state, we calculate the field patterns of the eigenmodes near the Dirac-like point with a small  $k$  along  $\Gamma X$  direction shown in Figs. 1(d)–(f). Figs. 1(d) and 1(e) show that the linear bands are linear combinations of the monopole and transverse dipole with its magnetic field polarized perpendicular to the wave vector, while the flat band corresponds to quasi-longitudinal dipole excitations with its magnetic field polarized parallel to the wave vector (shown in Fig. 1(f)). The existence of linear bands at the  $\Gamma$  point can be proved by using multiple scattering theory [49], tight-binding method [64–67] or k.p perturbation [58, 68]. It was shown that if the band dispersions in a 2D photonic crystal can be described by monopole and dipole excitations, an effective medium theory [69] can be applied to extract effective constitutive parameters of this 2D photonic crystal. The effective permittivity ( $\varepsilon_{eff}$ ) and permeability ( $\mu_{eff}$ ) as functions of frequency are shown in Fig. 1(b). We can see that  $\varepsilon_{eff}$  and  $\mu_{eff}$  indeed intersect at zero at the Dirac-like point frequency.

In order to demonstrate that the photonic crystal with a band dispersion shown in Fig. 1(a) does behave as if  $\varepsilon_{eff}(\omega_D) = \mu_{eff}(\omega_D) = 0$

at the Dirac-like point frequency, numerical simulations and microwave experiments were carried out [49]. Instead of using  $\epsilon = 12.5$ , we chose the alumina rods with  $\epsilon = 8.8$  for the experiment as these alumina rods are readily available. Fig. 2(a) shows that the measured field distributions of an incident plane wave illuminating from the left side onto a photonic crystal with a  $40 \times 40$  mm metallic obstacle imbedded inside. The exit waves on the right side preserve its plane wave front with little distortion as if the obstacle was not there. For comparison, we show the numerical simulated field distributions for a homogenous  $\epsilon = \mu = 0$  medium with a thin layer of air between the homogenous  $\epsilon = \mu = 0$  medium and the metallic block (shown in Fig. 2(b)). The

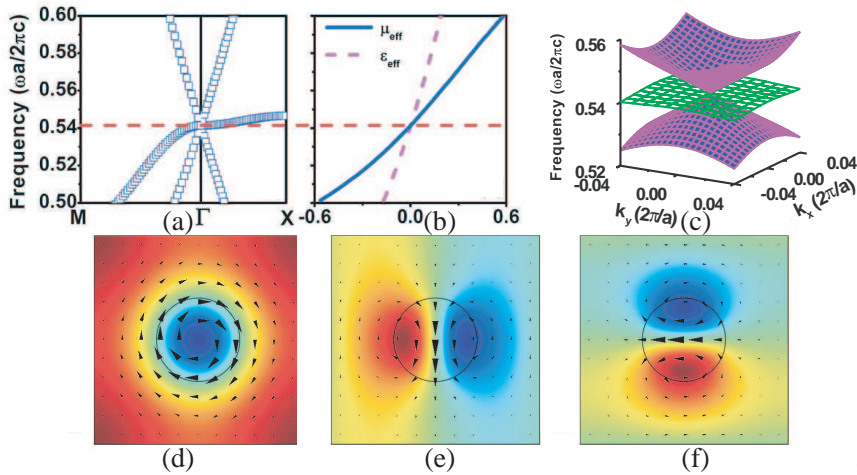


**Figure 1.** (a) The band structure for a 2D photonic crystal consisting of dielectric cylinders with radius  $R = 0.2a$ , relative permittivity  $\epsilon = 12.5$  and permeability  $\mu = 1$ . Here,  $a$  is the lattice constant. (b) The effective permittivity  $\epsilon_{eff}$  (pink dashed line) and permeability  $\mu_{eff}$  (blue solid line) as a function of frequency for the 2D photonic crystal. Note that  $\epsilon_{eff} = \mu_{eff} = 0$  at the Dirac-like point. (c) Three-dimensional dispersion surfaces near the Dirac-like point frequency of the band structure shown in (a), showing the relationship between the frequency and wave vectors ( $k_x$  and  $k_y$ ). (d)–(f) The field patterns of the eigenmodes near the Dirac-like point with a very small  $k$  along  $\Gamma X$  direction. The color patterns show the  $Ez$  fields and the vector fields show  $H$  fields. (d) The real part of  $Ez$  and the imaginary part of  $H$  at the frequency  $0.527c/a$ . (e) The imaginary part of the  $Ez$  and the real part of  $H$  at the frequency  $0.527c/a$ . (f) The real part of  $Ez$  and the imaginary part of  $H$  at the frequency  $0.541c/a$ .

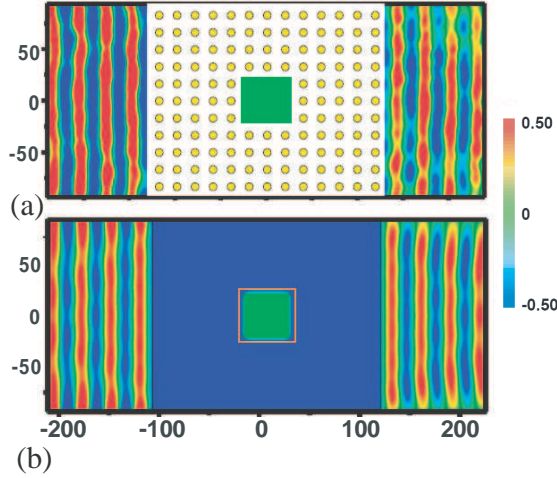


**Figure 2.** Simulation and microwave experiment to illustrate the “cloaking” effect of a zero-index medium. (a) The microwave experimental  $E_z$  field distributions observed at 10.3 GHz with a photonic crystal containing a  $40 * 40$  mm metallic obstacle (green) embedded in it. The incident plane wave comes from the left. The photonic crystal is a square array of alumina cylinders (each rod in yellow) with relative permittivity  $\varepsilon = 8.8$  and permeability  $\mu = 1$ . (b) Simulated  $E_z$  field distributions for a hypothetical homogenous  $\varepsilon = \mu = 0$  medium (blue) with a thin layer of air (between the orange boundary and the metallic block (green)) between the homogenous  $\varepsilon = \mu = 0$  medium and the metallic block (green).

exit fields still keep its plane wave front with little distortion. The field distributions between the experiment and simulation are consistent with each other.

### 3. 3D DIRAC-LIKE POINT IN PHOTONIC SYSTEM

After introducing the 2D Dirac-like point in photonic system, we will attempt to extend the concept of 2D Dirac-like to 3D. It is well known that photonic bands have quadratic dispersions at the  $\Gamma$  point as a consequence of time reversal symmetry. In order to illustrate the typical dispersion of a simple cubic lattice near the zone center, we calculate the photonic band structure of dielectric spheres arranged in a simple cubic lattice, which is shown in Fig. 3. The permittivity and permeability of the spheres are chosen to be  $\varepsilon = 12$  and  $\mu = 1$ . The radius is  $R = 0.3a$ , with  $a$  being the lattice constant. In the

frequency range of interest, the bands are derived from electric and magnetic dipolar excitations. There are two triply-degenerate states at  $\Gamma$  point and these states have different frequencies. The lower bands correspond to magnetic dipole modes which are labeled as  $T_{1u}$  at  $\vec{k} = 0$ , and the higher bands are the electric dipole modes labeled as  $T_{1g}$  at  $\vec{k} = 0$  [70]. Both sets of the bands have quadratic dispersions at the  $\Gamma$  point as expected. We cannot obtain linear dispersion at  $\Gamma$  point unless there is accidental degeneracy. However, in photonic crystals composing of the dielectric spheres arranged in a simple cubic lattice, it is very difficult, if not impossible, to make the  $T_{1u}$  and  $T_{1g}$  modes touch each other at the same frequency through tuning the filling ratio or permittivity of the spheres. To achieve accidental degeneracy, we need one more degree of freedom to tune the frequencies of these two modes. For that purpose, we employ a core-shell structure. The inset in Fig. 4(a) is the illustration of the simple cubic unit cell. The core (orange color in the figure) is a perfect electric conductor, the radius of which is  $R_1 = 0.102a$ . The shell (gray color in the figure) is dielectric with  $\epsilon = 12$  and  $\mu = 1$ . The outer radius of the shell is  $R_2 = 0.3a$ . The photonic band structure of these core-shell spheres arranged in a simple cubic lattice is shown in Fig. 4(a). With the extra degree of freedom allowed in a core-shell configuration, it is not difficult to find parameters so that the  $T_{1u}$  and  $T_{1g}$  modes touch each other at  $\Gamma$  point. For the system shown in Fig. 4, the accidental degeneracy occurs at the frequency  $f_D = 0.523c/a$ . As the electric and magnetic dipoles are

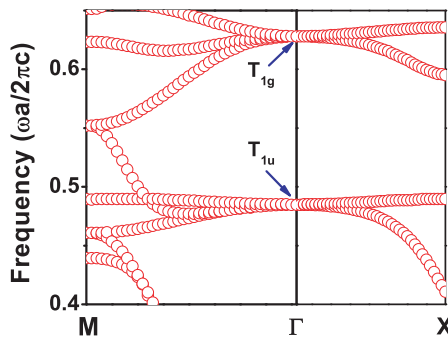


**Figure 3.** The photonic band structure of dielectric spheres arranged in a simple cubic lattice. The permittivity ( $\epsilon$ ) and permeability ( $\mu$ ) of the sphere are  $\epsilon = 12$ ,  $\mu = 1$ . The radius of it is  $R = 0.3a$ . Here,  $a$  is the lattice constant. We note that the triply degenerate  $T_{1g}$  and  $T_{1u}$  modes have different frequencies and the dispersions are quadratic near the zone center.

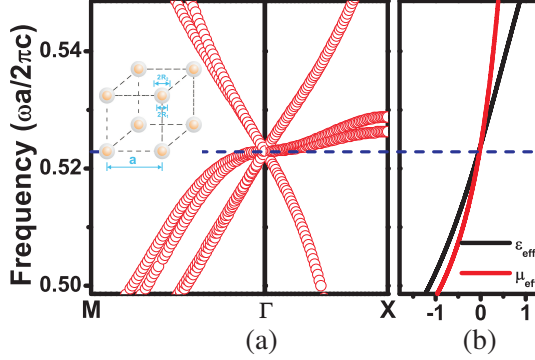


**Figure 4.** (a) The band structure of three dimensional core-shell photonic crystals with a simple cubic lattice. The inset is an illustration of the simple cubic unit cell. The cores (orange color) are made of perfect electric conductors, with radii of  $R_1 = 0.102a$ . The permittivity ( $\varepsilon$ ) and permeability ( $\mu$ ) of the dielectric shell (gray color) are  $\varepsilon = 12$ ,  $\mu = 1$ . The radius of the outer shell is  $R_2 = 0.3a$ . Here,  $a$  is the lattice constant. (b) The effective permittivity ( $\varepsilon_{eff}$ ) and permeability ( $\mu_{eff}$ ) as a function of frequency for this core-shell photonic crystal obtained using effective medium theory. The blue dash line marks the frequency of the Dirac-like point ( $f_D = 0.523c/a$ ) in the band structure. This coincides with the frequency at which  $\varepsilon_{eff} = \mu_{eff} = 0$ . In this case, the  $T_{1g}$  and  $T_{1u}$  modes are accidentally degenerate, giving rise to linear dispersions near the zone center for four of the bands.

each three-fold degenerate at  $\vec{k} = 0$ , the accidental degeneracy gives rise to a six-fold degenerate state at  $\Gamma$  point. Four bands have linear dispersions near the  $\Gamma$  point, the other two bands are relatively flat.

To visualize the accidental degeneracy further, we calculate the band structure of the core-shell spheres with different radii of the cores. The outer radius of the shell is kept constant ( $R_2 = 0.3a$ ). The photonic band structures for  $R_1 = 0.08a$  and  $R_1 = 0.12a$  are shown in Figs. 5(a) and 5(b), respectively. The six-fold degenerate state (shown in Fig. 4(a)) breaks into two triply-degenerate states. When  $R_1$  is smaller than  $0.102a$ , the frequency of  $T_{1u}$  mode is lower than that of  $T_{1g}$  mode. If  $R_1$  is bigger than  $0.102a$ ,  $T_{1u}$  mode becomes the higher frequency mode. It is quite obvious that by changing the radius of the core, the  $T_{1u}$  and  $T_{1g}$  modes will cross each other at the same frequency, which is consistent with the result shown in Fig. 4(a). Fig. 5 also shows that unless  $T_{1u}$  and  $T_{1g}$  modes coincide in frequency, the dispersion remains quadratic as in the case of simple dielectric

spheres shown in Fig. 3.

To prove the existence of the linear dispersion near the  $\Gamma$  point, we extend the method introduced by Sakoda in Ref. [64] to the more complicated case of six-fold degeneracy. We will use the same notation introduced in Ref. [64]. The secular equation of this 3D accidental-degeneracy-induced Dirac point (ADIDP) is:

$$\left| \mathbf{B} - \frac{\omega_k^2}{c^2} \mathbf{I} \right| = 0. \tag{1}$$

Here,  $\mathbf{I}$  is the unit matrix.  $\omega_k$  is the eigen frequency. The elements ( $B_{ij}$ ) of  $\mathbf{B}$  is defined by:

$$B_{ij} = \sum_{lmn} e^{ia(k_x l + k_y m + k_z n)} L_{lmn}^{(ij)} \tag{2}$$

Here,  $l, m, n$  are integers,  $k_x, k_y, k_z$  the Cartesian components of the Bloch wave vector, and  $L_{lmn}^{(ij)}$  the “electromagnetic transfer integrals” in 3D. By substituting the expressions of  $L_{lmn}^{(ij)}$  into Eq. (2), we can obtain the formulas of  $B_{ij}$ , which allows us to solve Eq. (1). The detailed derivations of the secular equation,  $L_{lmn}^{(ij)}$ , and  $B_{ij}$  are shown in the appendix. After some tedious calculations, we can solve Eq. (1)

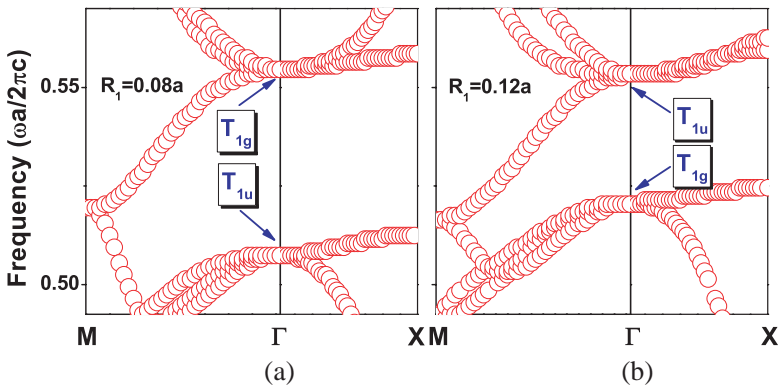


**Figure 5.** The band structure of three dimensional core-shell photonic crystals with simple cubic lattice for different radii of the cores ( $R_1$ ). The permittivity ( $\epsilon$ ) and permeability ( $\mu$ ) of the shell are  $\epsilon = 12, \mu = 1$ . The radius of it is  $R_2 = 0.3a$ . The cores are perfect electric conductors, the radii of the cores are (a)  $R_1 = 0.08a$  and (b)  $R_1 = 0.12a$ . Here,  $a$  is the lattice constant.

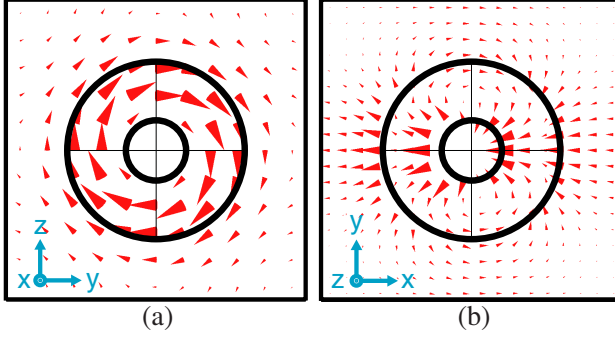


**Figure 6.** The electric fields of the eigenstates at the Dirac-like point frequency. The arrows show the directions of the electric field, the sizes of the arrows are proportional to the field amplitude. (a) The electric field in the  $yz$  plane ( $x = 0$  plane). The field pattern shows that the eigenmode is a magnetic dipole pointing along the  $x$  direction. (b) The electric field in the  $xy$  plane ( $z = 0$  plane), implying an electric dipole excitation in  $x$  direction.

to obtain the dispersion of the 3D ADIDP.

$$\omega_k = \begin{cases} \omega_\Gamma + |M_3| a c^2 k / \omega_\Gamma - \left( \frac{1}{12} (M'_1 + 2M''_1 + M'_2 + 2M''_2) / \omega_\Gamma \right. \\ \left. - \frac{1}{2\omega_\Gamma^3} c^2 |M_3|^2 \right) a^2 c^2 k^2 & \text{(double roots)} \\ \omega_\Gamma - |M_3| a c^2 k / \omega_\Gamma - \left( \frac{1}{12} (M'_1 + 2M''_1 + M'_2 + 2M''_2) / \omega_\Gamma \right. \\ \left. - \frac{1}{2\omega_\Gamma^3} c^2 |M_3|^2 \right) a^2 c^2 k^2 & \text{(double roots)} \\ \omega_\Gamma - \frac{1}{12} (M'_1 + 2M''_1 + M'_2 + 2M''_2) a^2 c^2 k^2 / \omega_\Gamma & \text{(double roots)} \end{cases} \quad (3)$$

Eq. (3) implies that in the band structure four bands have linear dispersions near the zone center, and the other two are quadratic in  $k$  in the lowest order. The dispersions are isotropic near  $\vec{k} = 0$ . This is consistent with the numerical results shown in the band structure in Fig. 4(a). The equi-frequency surfaces for the linear bands are spheres with radii proportional to the  $(\omega - \omega_D)$ .

In order to understand the underlying physics of this 3D ADIDP, we calculate the electric field patterns of the eigenstates at the Dirac-like point frequency ( $0.523c/a$ ). Fig. 6(a) demonstrates the electric field pattern in the  $yz$  plane ( $x = 0$  plane). The arrows show

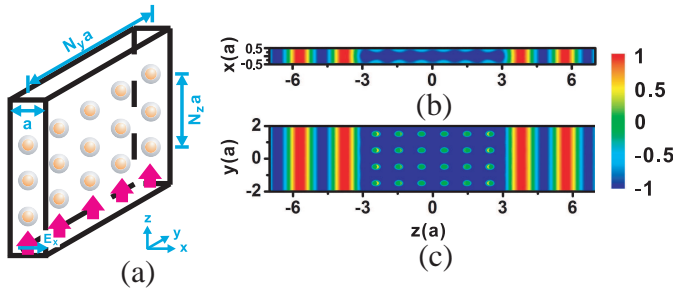


**Figure 7.** Finite-difference time-domain simulations showing that waves can go through the core-shell photonic crystal with very small distortions of wavefront, as expected from a  $\epsilon_{eff} = \mu_{eff} = 0$  material. (a) The super cell used for the simulations. Periodical boundary conditions are applied to the side walls ( $xz$ , and  $yz$  planes). Perfectly matched layer boundary conditions are applied at the top and bottom walls ( $xy$  planes). There is only one unit cell in the  $x$  direction and there are  $N_y$  unit cells in the  $y$  direction. The thickness of the sample has  $N_z$  unit cells. In the simulations,  $N_y = 4$ ,  $N_z = 6$ . The core-shell spheres are arranged from  $-1.5a$  to  $1.5a$  and  $-2.5a$  to  $2.5a$  along  $y$  and  $z$  directions. The plane waves are incident from the negative  $z$  direction (as indicated by the pink arrows) with the electric field polarized along  $x$  direction (blue arrows). (b) the electric field pattern in the  $xz$  plane ( $y = 0$  plane), and (c) the electric field pattern in the  $yz$  plane ( $x = 0$  plane).

the directions of the electric field, the sizes of the arrows show the amplitude of the field. The field pattern shows that this eigenstate is a magnetic dipole pointing along the  $x$  direction. Fig. 6(b) shows the electric field pattern in the  $xy$  plane ( $z = 0$  plane), which looks like an electric dipole. The eigenstates of the other four modes at the Dirac-like point frequency correspond to magnetic and electric dipole excitations along  $y$  and  $z$  directions (not shown here). Therefore, the 3D ADIDP can be described by electric and magnetic dipole excitations along  $x$ ,  $y$ , and  $z$  directions.

We have shown previously that in 2D photonic crystals, Dirac-like points that are derived from the accidentally degeneracy of monopole and dipole excitations can be mapped to a zero-refractive-index at that frequency [49]. Is it possible to describe the Dirac-like point physics in 3D with effective medium theory? We apply the effective medium theory shown in Ref. [69] to calculate the effective medium of this 3D ADIDP. The effective permittivity ( $\epsilon_{eff}$ ) and permeability ( $\mu_{eff}$ ) as a function of frequency are shown in Fig. 4(b). At the 3D Dirac-like

point frequency, effective medium theory found that  $\varepsilon_{eff} = \mu_{eff} = 0$ . That is to say, the core-shell simple cubic structure will behave as if it is an isotropic system with  $\varepsilon_{eff} = \mu_{eff} = 0$  at the Dirac-like point frequency. This is different from the case of 2D Dirac-like cone systems which are anisotropic and as such, can only give zero refractive index only for one polarization.

Zero-index material has many interesting wave manipulating properties [24–39]. We perform finite-difference time-domain simulations to see whether our core-shell structure has properties similar to a zero-index material. Fig. 7 shows a snapshot of field patterns of incident plane waves going through the core-shell photonic crystal. Due to the limitation of computation resources, we use a relatively small super cell to do the simulations (shown in Fig. 7(a)). The side walls ( $xz$ , and  $yz$  planes) have periodical boundary conditions. There is only one unit cell in the  $x$  direction, while there are  $N_y$  unit cells in the  $y$  direction. Perfectly matched layer boundary conditions are imposed on the top and bottom walls ( $xy$  planes). The sample is  $N_z$  unit cells thick in the  $z$  direction. In our simulations shown, we use  $N_y = 4$ ,  $N_z = 6$ . The core-shell spheres are arranged from  $-1.5a$  to  $1.5a$  and  $-2.5a$  to  $2.5a$  in the  $y$  and  $z$  directions. The incident plane waves come in from the negative  $z$  direction as indicated by the pink arrows in the figure with the polarization of the electric field along the  $x$  direction (blue arrows). In Fig. 7(b), the electric field pattern in the  $xz$  plane ( $y = 0$  plane) preserves its plane wave front without distortion. In  $yz$  plane ( $x = 0$  plane), the electric field pattern also preserves its plane wave front (shown in Fig. 7(c)). Examining the field patterns inside the core-shell photonic crystal (shown in Figs. 7(b) and 7(c)), we can find little phase inside the photonic crystal, which is expected if the material has  $\varepsilon_{eff} = \mu_{eff} = 0$ .

#### 4. 3D DIRAC-LIKE POINT IN PHONONIC SYSTEM

From the previous discussions, we see that 3D ADIDP in photonic systems can be achieved with the accidental degeneracy of electric and magnetic dipoles resulting in a six-fold degenerate Dirac-like point at the zone center. We are going to show below that the scheme proposed in Ref. [64], using  $A_{1g}$  (one-fold) and  $T_{1u}$  modes (three-fold) to get 3D Dirac-like point, can actually be employed in acoustic wave systems rather than in photonic systems. We calculate the band structure of 3D simple cubic lattice acoustic crystals consisting of rubber spheres in water. The radius of rubber is  $R = 0.255a$ , with  $a$  being the lattice constant. The density of rubber is taken to be  $\rho = 1.3 \times 10^3 \text{ kg/m}^3$ , and that of water is  $\rho_0 = 1.0 \times 10^3 \text{ kg/m}^3$ . The Lamé constant in rubber is

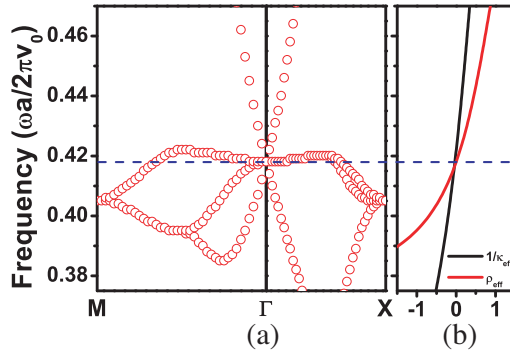


**Figure 8.** (a) The band structure of three dimensional simple cubic acoustic crystals consisting of rubber spheres (radius  $R = 0.255a$ ) in water. Here,  $a$  is the lattice constant. The density of rubber is taken to be  $\rho = 1.3 \times 10^3 \text{ kg/m}^3$ , and that of water is  $\rho_0 = 1.0 \times 10^3 \text{ kg/m}^3$ . The Lamé constant in rubber is  $\kappa = 1.17 \times 10^8 \text{ N/m}^2$  and for water  $\kappa_0 = 2.22 \times 10^9 \text{ N/m}^2$ . (b) The effective mass density ( $\rho_{eff}$ ) and reciprocal of bulk modulus ( $1/\kappa_{eff}$ ) as a function of frequency obtained using effective medium theory for this simple cubic phononic crystal. The blue dash line marks the frequency of the Dirac-like point ( $f_D = 0.418v_0/a$ ) in the band structure which coincides with the frequency at which  $\rho_{eff} = 1/\kappa_{eff} = 0$  in the effective medium.

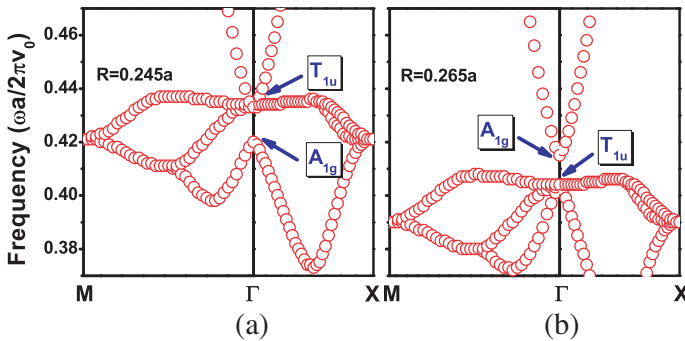


**Figure 9.** The band structure of three dimensional acoustic crystals arranged in a simple cubic lattice for different radii ( $R$ ).  $R = 0.245a$  for Fig. 9(a), and  $R = 0.265a$  for Fig. 9(b). Here,  $a$  is the lattice constant. The density of rubber is taken to be  $\rho = 1.3 \times 10^3 \text{ kg/m}^3$ , and that of water is  $\rho_0 = 1.0 \times 10^3 \text{ kg/m}^3$ . The Lamé constant in rubber is  $\kappa = 1.17 \times 10^8 \text{ N/m}^2$  and for water  $\kappa_0 = 2.22 \times 10^9 \text{ N/m}^2$ .

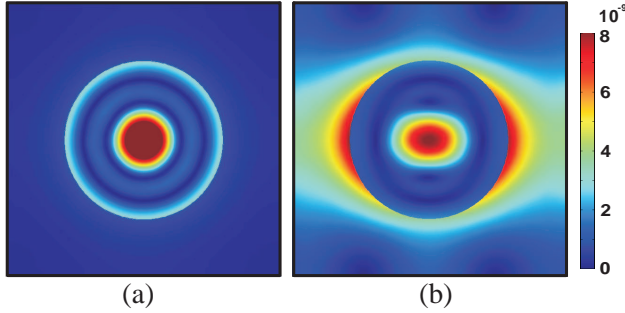


**Figure 10.** The displacement field patterns of the eigenstates at the Dirac-like point frequency ( $f_D = 0.418v_0/a$ ). (a) Implies a monopolar. (b) Implies a dipolar.

taken to be  $\kappa = 1.17 \times 10^8 \text{ N/m}^2$  and for water  $\kappa_0 = 2.22 \times 10^9 \text{ N/m}^2$ . For simplicity, we have ignored the shear wave within the rubber spheres due to the high velocity contrast between the rubber and water, and the main features will stay the same if we also include the shear wave within the spheres [71]. Fig. 8(a) shows a four-fold degenerate state at the  $\Gamma$  point at a frequency  $f_D = 0.418v_0/a$ . Here,  $v_0$  is the acoustic velocity of water. Two bands have linear dispersions near  $\vec{k} = 0$ , and the other two have quadratic dispersions. For the linear bands, the equi-frequency surfaces are spheres with radii proportional to  $(\omega - \omega_D)$ . This Dirac-like point is also induced by accidental degeneracy. However, it is obviously different from the 3D ADIDP in the photonic system, which is six-fold degenerate. To visualize the accidental degeneracy further, we calculate the band structure of the acoustic crystal with different radii (shown in Fig. 9) of the rubber spheres. The four-fold degenerate state now breaks into a singly-degenerate state ( $A_{1g}$  mode) and a triply-degenerate state ( $T_{1u}$  mode), both with zero group velocity at the zone center. When the radius is smaller than  $0.255a$  (the radius satisfies the 3D Dirac-like point condition), the frequency of the singly-degenerate state is lower than the triply-degenerate state (Fig. 9(a)). If the radius is bigger than  $0.255a$ , the ordering reverses (Fig. 9(b)). The ordering of the states for spheres with different radii implies that at certain radius, these two modes will touch each other at the same frequency, which is consistent with the results shown in Fig. 8(a). To understand the underlying physics, we calculate the displacement field pattern of the eigenstates at the Dirac-like point frequency shown in Fig. 10. The displacement patterns in Figs. 10(a) and 10(b) are consistent with a monopole and dipole excitation, respectively. The monopole and

dipole modes correspond to the  $A_{1g}$  and  $T_{1u}$  modes. The existence of the 3D ADIDP in this acoustic crystal with four degrees of freedom can be proved with the method shown in Ref. [64].

Using effective medium theory [72], we can calculate the effective mass density ( $\rho_{eff}$ ) and reciprocal of bulk modulus ( $1/\kappa_{eff}$ ) of this acoustic crystal. The effective mass density and reciprocal of bulk modulus are simultaneously equal to zero at the frequency  $0.418v_0/a$ . This frequency is the same as the Dirac-like point frequency in the band structure. We note that in 2D geometries, acoustic systems with Dirac-like point derived from the accidental degeneracy of monopole and dipole excitations can be mapped to a zero-index effective medium [50]. The results here show that the same analogy exists for Dirac-like points in 3D derived from  $A_{1g}$  and  $T_{1u}$  degeneracy.

## 5. SUMMARY

In summary, we show that a Dirac-like point formed by a triply-degenerate state can exist at the  $\Gamma$  point in 2D photonic crystal. Such triply-degenerate states are consequences of accidental degeneracy, which can be achieved by tuning system parameters. For the triply-degenerate state are derived from monopole and dipole excitations, the system can be mapped to  $\varepsilon_{eff} = \mu_{eff} = 0$  material through effective medium theory. We then extend the 2D Dirac-like point concept to 3D. We proposed physically realizable structures to obtain 3D ADIDP in both photonic and phononic systems. The Dirac-like point in 3D photonic systems is a six-fold degenerate state, formed by the accidental degeneracy of electric and magnetic dipoles excitations, while in the acoustic wave system it is a four-fold degenerate state, formed by the monopole and dipole excitations. In the photonic case, we find that we can use core-shell systems to achieve the accidental degeneracy. Using effective medium theories, we can map these structures to a material with effective permittivity and permeability simultaneously equal to zero in the photonic system, and with effective mass density and reciprocal of bulk modulus simultaneously equal to zero in the phononic system. These systems are platforms that enable us to extend the notion of “Dirac points” from 2D to 3D. As the density of states near the 3D Dirac points are different from those near 2D Dirac points, new transport properties may emerge from those systems. These would be interesting topics for further studies. In 2D systems with Dirac-like cones at the zone center, only some components in the constitutive relationship are zero. In 3D, all components are zero at the Dirac-like point. As “zero-index” effective media, they are probably more interesting than their 2D counterparts.

## ACKNOWLEDGMENT

The work is supported by Hong Kong Research Grant Council GRF grant 600311.

## APPENDIX A.

In this appendix, we extend the method introduced by Sakoda in Ref. [64] to show the existence of the 3D ADIDP in the simple cubic photonic crystal with core-shell spheres. We will use the same notations as Ref. [64]. The 3D ADIDP is a six-fold degenerate state, comprising the  $T_{1u}$  and  $T_{1g}$  modes. The eigen fields of the 3D ADIDP near  $\Gamma$  point ( $\vec{H}_k(\vec{r})$ ) can be described by the linear combination of the basis functions with the same symmetry as the  $T_{1u}$  and  $T_{1g}$  modes.

$$\vec{H}_k(\vec{r}) = \frac{1}{V} \sum_{l,m,n} e^{i\vec{k}\cdot\vec{r}_{lmn}} \sum_{i=1}^6 A_i \vec{H}^{(i)}(\vec{r} - \vec{r}_{lmn}) \quad (\text{A1})$$

Here,  $V$  is the volume of the unit cell,  $\vec{r}_{lmn} = l \begin{pmatrix} a \\ 0 \\ 0 \end{pmatrix} + m \begin{pmatrix} 0 \\ a \\ 0 \end{pmatrix} + n \begin{pmatrix} 0 \\ 0 \\ a \end{pmatrix}$  is a lattice vector of the simple cubic structure, and  $l, m, n$

are integer.  $A_i$  is the coefficient of the linear combination.  $\vec{k}$  is Bloch wave vector.  $\vec{H}^{(i)}(\vec{r})$  is the basis function comprising  $T_{1u}$  or  $T_{1g}$  modes. The indices  $i = 1, 2, 3$  represent the  $T_{1u}$  mode, and  $i = 4, 5, 6$  for  $T_{1g}$  mode. From the Maxwell equation, the eigenvalue equation is given by:

$$\mathcal{L}\vec{H}_k(\vec{r}) = \frac{\omega_k^2}{c^2} \vec{H}_k(\vec{r}) \quad (\text{A2})$$

Here,  $\mathcal{L} = \nabla \times (\frac{1}{\varepsilon(\vec{r})} \nabla \times)$ .  $\varepsilon(\vec{r})$  is the permittivity. The eigenfrequency is given by  $\omega_k$ . The electromagnetic transfer integral in three dimensions can be defined by:

$$L_{lmn}^{(ij)} = \frac{1}{V} \int d\vec{r} \vec{H}^{(i)*}(\vec{r}) \cdot \mathcal{L}\vec{H}^{(j)}(\vec{r} - \vec{r}_{lmn}) \quad (\text{A3})$$

Using symmetry, we can obtain the functional form of  $L_{lmn}^{(ij)}$  through Eq. (A3). In this process, we will use the symmetry operator to operate onto the eigen fields ( $\vec{H}^{(i)}(\vec{r})$ ) of  $T_{1u}$  and  $T_{1g}$  modes.

The matrix representations of  $T_{1u}$  mode are already shown in Ref. [64]. For ease of reference, we write down some of them again in the following.

$$\begin{aligned} \sigma_x &: \begin{pmatrix} -1 & 0 & 0 \\ 0 & 1 & 0 \\ 0 & 0 & 1 \end{pmatrix}; \quad \sigma_y : \begin{pmatrix} 1 & 0 & 0 \\ 0 & -1 & 0 \\ 0 & 0 & 1 \end{pmatrix}; \quad \sigma_z : \begin{pmatrix} 1 & 0 & 0 \\ 0 & 1 & 0 \\ 0 & 0 & -1 \end{pmatrix}; \\ C_{4x} &: \begin{pmatrix} 1 & 0 & 0 \\ 0 & 0 & 1 \\ 0 & -1 & 0 \end{pmatrix}; \quad C_{4y} : \begin{pmatrix} 0 & 0 & -1 \\ 0 & 1 & 0 \\ 1 & 0 & 0 \end{pmatrix}; \quad C_{4z} : \begin{pmatrix} 0 & 1 & 0 \\ -1 & 0 & 0 \\ 0 & 0 & 1 \end{pmatrix}; \\ C_{4x}^{-1} &: \begin{pmatrix} 1 & 0 & 0 \\ 0 & 0 & -1 \\ 0 & 1 & 0 \end{pmatrix}; \quad C_{4y}^{-1} : \begin{pmatrix} 0 & 0 & 1 \\ 0 & 1 & 0 \\ -1 & 0 & 0 \end{pmatrix}; \quad C_{4z}^{-1} : \begin{pmatrix} 0 & -1 & 0 \\ 1 & 0 & 0 \\ 0 & 0 & 1 \end{pmatrix}; \\ C_{3(111)} &: \begin{pmatrix} 0 & 1 & 0 \\ 0 & 0 & 1 \\ 1 & 0 & 0 \end{pmatrix}; \quad C_{3(111)}^{-1} : \begin{pmatrix} 0 & 0 & 1 \\ 1 & 0 & 0 \\ 0 & 1 & 0 \end{pmatrix}; \end{aligned}$$

The polynomial representation of  $T_{1g}$  mode is given by  $\{yz(y^2 - z^2), zx(z^2 - x^2), xy(x^2 - y^2)\}$  [68]. The matrix representations are shown below.

$$\begin{aligned} \sigma_x &: \begin{pmatrix} 1 & 0 & 0 \\ 0 & -1 & 0 \\ 0 & 0 & -1 \end{pmatrix}; \quad \sigma_y : \begin{pmatrix} -1 & 0 & 0 \\ 0 & 1 & 0 \\ 0 & 0 & -1 \end{pmatrix}; \quad \sigma_z : \begin{pmatrix} -1 & 0 & 0 \\ 0 & -1 & 0 \\ 0 & 0 & 1 \end{pmatrix}; \\ C_{4x} &: \begin{pmatrix} 1 & 0 & 0 \\ 0 & 0 & 1 \\ 0 & -1 & 0 \end{pmatrix}; \quad C_{4y} : \begin{pmatrix} 0 & 0 & -1 \\ 0 & 1 & 0 \\ 1 & 0 & 0 \end{pmatrix}; \quad C_{4z} : \begin{pmatrix} 0 & 1 & 0 \\ -1 & 0 & 0 \\ 0 & 0 & 1 \end{pmatrix}; \\ C_{4x}^{-1} &: \begin{pmatrix} 1 & 0 & 0 \\ 0 & 0 & -1 \\ 0 & 1 & 0 \end{pmatrix}; \quad C_{4y}^{-1} : \begin{pmatrix} 0 & 0 & 1 \\ 0 & 1 & 0 \\ -1 & 0 & 0 \end{pmatrix}; \quad C_{4z}^{-1} : \begin{pmatrix} 0 & -1 & 0 \\ 1 & 0 & 0 \\ 0 & 0 & 1 \end{pmatrix}; \\ C_{3(111)} &: \begin{pmatrix} 0 & 1 & 0 \\ 0 & 0 & 1 \\ 1 & 0 & 0 \end{pmatrix}; \quad C_{3(111)}^{-1} : \begin{pmatrix} 0 & 0 & 1 \\ 1 & 0 & 0 \\ 0 & 1 & 0 \end{pmatrix}; \end{aligned}$$

According to Eq. (A3), we calculate  $L_{lmn}^{(ij)}$  for  $T_{1u}$  mode [64].

$$\begin{aligned} L_{000}^{(11)} &= L_{000}^{(22)} = L_{000}^{(33)} = \frac{\omega_1^2}{c^2} + M_1 \\ L_{\pm 1,00}^{(11)} &= L_{0,\pm 1,0}^{(22)} = L_{00,\pm 1}^{(33)} = M_1' \\ L_{0,\pm 1,0}^{(11)} &= L_{00,\pm 1}^{(11)} = L_{\pm 1,00}^{(22)} = L_{00,\pm 1}^{(22)} = L_{\pm 1,00}^{(33)} = L_{0,\pm 1,0}^{(33)} = M_1'' \\ L_{000}^{(12)} &= L_{000}^{(21)} = L_{000}^{(13)} = L_{000}^{(31)} = L_{000}^{(23)} = L_{000}^{(32)} = 0 \end{aligned}$$

$$\begin{aligned}
L_{\pm 1,00}^{(12)} &= L_{0,\pm 1,0}^{(12)} = L_{00,\pm 1}^{(12)} = L_{\pm 1,00}^{(21)} = L_{0,\pm 1,0}^{(21)} = L_{00,\pm 1}^{(21)} = L_{\pm 1,00}^{(13)} \\
&= L_{0,\pm 1,0}^{(13)} = L_{00,\pm 1}^{(13)} = L_{\pm 1,00}^{(31)} = L_{0,\pm 1,0}^{(31)} = L_{00,\pm 1}^{(31)} = L_{\pm 1,00}^{(23)} \\
&= L_{0,\pm 1,0}^{(23)} = L_{00,\pm 1}^{(23)} = L_{\pm 1,00}^{(32)} = L_{0,\pm 1,0}^{(32)} = L_{00,\pm 1}^{(32)} = 0
\end{aligned}$$

Here,  $\omega_1$  is the eigen frequency of  $T_{1u}$  mode.

Next, we give the expression for  $L_{lmn}^{(ij)}$  for  $T_{1g}$  mode. The results are very similar to the  $T_{1u}$  mode.

$$\begin{aligned}
L_{000}^{(44)} &= L_{000}^{(55)} = L_{000}^{(66)} = \frac{\omega_2^2}{c^2} + M_2 \\
L_{\pm 1,00}^{(44)} &= L_{0,\pm 1,0}^{(55)} = L_{00,\pm 1}^{(66)} = M_2' \\
L_{0,\pm 1,0}^{(44)} &= L_{00,\pm 1}^{(44)} = L_{\pm 1,00}^{(55)} = L_{00,\pm 1}^{(55)} = L_{\pm 1,00}^{(66)} = L_{0,\pm 1,0}^{(66)} = M_2'' \\
L_{000}^{(45)} &= L_{000}^{(54)} = L_{000}^{(46)} = L_{000}^{(64)} = L_{000}^{(56)} = L_{000}^{(65)} = 0 \\
L_{\pm 1,00}^{(45)} &= L_{0,\pm 1,0}^{(45)} = L_{00,\pm 1}^{(45)} = L_{\pm 1,00}^{(54)} = L_{0,\pm 1,0}^{(54)} = L_{00,\pm 1}^{(54)} \\
&= L_{\pm 1,00}^{(46)} = L_{0,\pm 1,0}^{(46)} = L_{00,\pm 1}^{(46)} = L_{\pm 1,00}^{(64)} = L_{0,\pm 1,0}^{(64)} = L_{00,\pm 1}^{(64)} = L_{\pm 1,00}^{(56)} \\
&= L_{0,\pm 1,0}^{(56)} = L_{00,\pm 1}^{(56)} = L_{\pm 1,00}^{(65)} = L_{0,\pm 1,0}^{(65)} = L_{00,\pm 1}^{(65)} = 0
\end{aligned}$$

Here,  $\omega_2$  is the eigen frequency of  $T_{1g}$  mode.

At last, we should consider the interaction terms between  $T_{1u}$  and  $T_{1g}$  modes. The results are shown in the following.

$$\pm L_{00,\pm 1}^{(15)} = \pm L_{0,\pm 1,0}^{(16)} = \pm L_{00,\mp 1}^{(24)} = \pm L_{\pm 1,00}^{(26)} = \pm L_{0,\pm 1,0}^{(34)} = \pm L_{\mp 1,00}^{(35)} = M_3$$

Using the relation  $L_{lmn}^{(ij)} = L_{-l,-m,-n}^{(ji)*}$ , we can obtain:

$$\pm L_{00,\mp 1}^{(51)} = \pm L_{0,\pm 1,0}^{(61)} = \pm L_{00,\pm 1}^{(42)} = \pm L_{\mp 1,00}^{(62)} = \pm L_{0,\mp 1,0}^{(43)} = \pm L_{\pm 1,00}^{(53)} = M_3^*$$

$M_3^*$  is the conjugate of  $M_3$ . The other interaction terms are equal to zero. The secular equation of Eq. (A2) is :

$$\left| \mathbf{B} - \frac{\omega_{\mathbf{k}}^2}{c^2} \mathbf{I} \right| = 0. \quad (\text{A4})$$

Here,  $\mathbf{I}$  is the unit matrix. The elements  $(B_{ij})$  of  $\mathbf{B}$  is defined by:

$$B_{ij} = \sum_{lmn} e^{ia(k_x l + k_y m + k_z n)} L_{lmn}^{(ij)}$$

To keep the mathematics manageable, we only consider nearest neighbor hopping. By substituting the expressions of  $L_{lmn}^{(ij)}$  into the

above equation, we obtain the expressions of  $B_{ij}$ .

$$B_{11} = \frac{\omega_1^2}{c^2} + M_1 + 2M'_1 \cos(k_x a) + 2M''_1 [\cos(k_y a) + \cos(k_z a)]$$

$$B_{15} = 2iM_3 \sin(k_z a)$$

$$B_{16} = -2iM_3 \sin(k_y a)$$

$$B_{22} = \frac{\omega_1^2}{c^2} + M_1 + 2M'_1 \cos(k_y a) + 2M''_1 [\cos(k_z a) + \cos(k_x a)]$$

$$B_{24} = -2iM_3 \sin(k_z a)$$

$$B_{26} = 2iM_3 \sin(k_x a)$$

$$B_{33} = \frac{\omega_1^2}{c^2} + M_1 + 2M'_1 \cos(k_z a) + 2M''_1 [\cos(k_x a) + \cos(k_y a)]$$

$$B_{34} = 2iM_3 \sin(k_y a)$$

$$B_{35} = -2iM_3 \sin(k_x a)$$

$$B_{42} = 2iM_3^* \sin(k_z a)$$

$$B_{43} = -2iM_3^* \sin(k_y a)$$

$$B_{44} = \frac{\omega_2^2}{c^2} + M_2 + 2M'_2 \cos(k_x a) + 2M''_2 [\cos(k_y a) + \cos(k_z a)]$$

$$B_{51} = -2iM_3^* \sin(k_z a)$$

$$B_{53} = 2iM_3^* \sin(k_x a)$$

$$B_{55} = \frac{\omega_2^2}{c^2} + M_2 + 2M'_2 \cos(k_y a) + 2M''_2 [\cos(k_z a) + \cos(k_x a)]$$

$$B_{61} = 2iM_3^* \sin(k_y a)$$

$$B_{62} = -2iM_3^* \sin(k_x a)$$

$$B_{66} = \frac{\omega_2^2}{c^2} + M_2 + 2M'_2 \cos(k_z a) + 2M''_2 [\cos(k_x a) + \cos(k_y a)]$$

$$B_{12} = B_{13} = B_{14} = B_{21} = B_{23} = B_{25} = B_{31} = B_{32} = B_{36} = B_{41}$$

$$= B_{45} = B_{46} = B_{52} = B_{54} = B_{56} = B_{63} = B_{64} = B_{65} = 0$$

Based on Eq. (A4), we use the notations

$$\xi = \frac{\omega_{\mathbf{k}}^2}{c^2}, \quad \xi_1 = \frac{\omega_1^2}{c^2}, \quad \xi_2 = \frac{\omega_2^2}{c^2}$$

Eq. (A4) is reduced to:

$$\xi^6 + b_5 \xi^5 + b_4 \xi^4 + b_3 \xi^3 + b_2 \xi^2 + b_1 \xi + b_0 = 0 \tag{A5}$$

At  $\Gamma$  point of the Brillouin zone, the solutions of Eq. (A5) are:

$$\xi = \begin{cases} \xi_1 + M_1 + 2M'_1 + 4M''_1 = \xi_{\Gamma}^{(1)} & \text{(triple roots)} \\ \xi_2 + M_2 + 2M'_2 + 4M''_2 = \xi_{\Gamma}^{(2)} & \text{(triple roots)} \end{cases}$$

If we change the form of  $\xi$  to  $\eta$  with the relation:

$$\eta = \xi + \frac{b_5}{6} \quad (\text{A6})$$

Therefore, Eq. (A5) can be changed to:

$$\eta^6 + p\eta^4 + q\eta^3 + r\eta^2 + s\eta + t = 0 \quad (\text{A7})$$

Here,

$$\begin{aligned} p &= b_4 - \frac{5}{12}b_5^2 \\ q &= b_3 - \left( \frac{5}{54}b_5^3 + \frac{2}{3}b_5p \right) \\ r &= b_2 - \left( \frac{5}{432}b_5^4 + \frac{1}{6}b_5^2p + \frac{1}{2}b_5q \right) \\ s &= b_1 - \left( \frac{1}{1296}b_5^5 + \frac{1}{54}b_5^3p + \frac{1}{12}b_5^2q + \frac{1}{3}b_5r \right) \\ t &= b_0 - \left( \frac{1}{46656}b_5^6 + \frac{1}{1296}b_5^4p + \frac{1}{216}b_5^3q + \frac{1}{36}b_5^2r + \frac{1}{6}b_5s \right) \end{aligned}$$

To evaluate the  $\vec{k}$  dependence of the eigen value equation around  $\Gamma$  point, we expand the parameters  $p, q, r, s, t$  in the second, third, fourth, fifth and sixth order of  $k_x, k_y, k_z$ , respectively.

For the accidental degeneracy of the  $T_{1u}$  and  $T_{1g}$  modes at  $\Gamma$  point,

$$\xi_{\Gamma}^{(1)} = \xi_{\Gamma}^{(2)} = \xi_{\Gamma}$$

Through very cumbersome calculations, we can obtain:

$$p = -8|M_3|^2 k^2 a^2 \quad r = 16|M_3|^4 k^4 a^4 \quad q = s = t = 0$$

where  $k = \sqrt{k_x^2 + k_y^2 + k_z^2}$ .

Since  $b_5 = -6\xi_{\Gamma} + (M'_1 + 2M''_1 + M'_2 + 2M''_2) k^2 a^2$ .

The solutions of Eq. (A5) are:

$$\xi = \begin{cases} \xi_{\Gamma} + 2|M_3|ka - \frac{1}{6}(M'_1 + 2M''_1 + M'_2 + 2M''_2)k^2a^2 & (\text{double roots}) \\ \xi_{\Gamma} - 2|M_3|ka - \frac{1}{6}(M'_1 + 2M''_1 + M'_2 + 2M''_2)k^2a^2 & (\text{double roots}) \\ \xi_{\Gamma} - \frac{1}{6}(M'_1 + 2M''_1 + M'_2 + 2M''_2)k^2a^2 & (\text{double roots}) \end{cases}$$

Since  $\omega_k = c\sqrt{\xi}$ , and  $\omega_\Gamma = c\sqrt{\xi_\Gamma}$ , we obtain the dispersion of the 3D ADIDP:

$$\omega_k = \begin{cases} \omega_\Gamma + |M_3| ac^2k/\omega_\Gamma - \left( \frac{1}{12} (M'_1 + 2M''_1 + M'_2 + 2M''_2) / \omega_\Gamma \right. \\ \left. - \frac{1}{2\omega_\Gamma^3} c^2 |M_3|^2 \right) a^2 c^2 k^2 & \text{(double roots)} \\ \omega_\Gamma - |M_3| ac^2k/\omega_\Gamma - \left( \frac{1}{12} (M'_1 + 2M''_1 + M'_2 + 2M''_2) / \omega_\Gamma \right. \\ \left. - \frac{1}{2\omega_\Gamma^3} c^2 |M_3|^2 \right) a^2 c^2 k^2 & \text{(double roots)} \\ \omega_\Gamma - \frac{1}{12} (M'_1 + 2M''_1 + M'_2 + 2M''_2) a^2 c^2 k^2 / \omega_\Gamma & \text{(double roots)} \end{cases}$$

## REFERENCES

1. Landau, L. and E. M. Lifschitz, *Electrodynamics of Continuous Media*, Elsevier, New York, 1984.
2. Veselago, V. G., "The electrodynamic of substances with simultaneously negative values of  $\epsilon$  and  $\mu$ ," *Soviet Physics Uspekhi*, Vol. 10, No. 4, 509–514, 1968.
3. Pendry, J. B., A. J. Holden, D. Robbins, and W. J. Stewart, "Magnetism from conductors and enhanced nonlinear phenomena," *IEEE Transactions on Microwave Theory and Techniques*, Vol. 47, No. 11, 2075–2084, 1999.
4. Shelby, R., D. R. Smith, and S. Schultz, "Experimental verification of a negative index of refraction," *Science*, Vol. 292, No. 5514, 77–79, 2001.
5. Smith, D. R., W. J. Padilla, D. C. Vier, S. C. Nemat-Nasser, and S. Schultz, "Composite medium with simultaneously negative permeability and permittivity," *Physical Review Letters*, Vol. 84, 4184–4187, 2000.
6. Zhang, S., W. Fan, N. C. Panoiu, K. J. Malloy, R. M. Osgood, and S. R. J. Brueck, "Experimental demonstration of near-infrared negative-index metamaterials," *Physical Review Letters*, Vol. 95, 137404, 2005.
7. Shalaev, V. M., W. Cai, U. K. Chettiar, H. K. Yuan, A. K. Sarychev, V. P. Drachev, and A. V. Kildishev, "Negative index of refraction in optical metamaterials," *Optics Letters*, Vol. 30, No. 24, 3356–3358, 2005.
8. Dolling, G., M. Wegener, C. M. Soukoulis, and S. Linden, "Negative-index metamaterial at 780 nm wavelength," *Optics Letters*, Vol. 32, No. 1, 53–55, 2007.

9. Pendry, J. B., "Negative refraction makes a perfect lens," *Physical Review Letters*, Vol. 85, 3966–3969, 2000.
10. Garcia, N. and M. Nieto-Vesperinas, "Left-handed materials do not make a perfect lens," *Physical Review Letters*, Vol. 88, 207403, 2002.
11. Grbic, A. and G. V. Eleftheriades, "Overcoming the diffraction limit with a planar left-handed transmission-line lens," *Physical Review Letters*, Vol. 92, 117403, 2004.
12. Parimi, P. V., W. T. Lu, P. Vodo, and S. Sridhar, "Imaging by flat lens using negative refraction," *Nature*, Vol. 426, 404, 2003.
13. Fang, N., H. Lee, C. Sun, and X. Zhang, "Sub-diffraction-limited optical imaging with a silver superlens," *Science*, Vol. 308, No. 5721, 534–537, 2005.
14. Chew, W. C., "Some reflections on double negative materials," *Progress In Electromagnetics Research*, Vol. 51, 1–26, 2005.
15. Pendry, J. B., D. Schurig, and D. R. Smith, "Controlling electromagnetic fields," *Science*, Vol. 312, No. 5781, 1780–1782, 2006.
16. Leonhardt, U., "Optical conformal mapping," *Science*, Vol. 312, No. 5781, 1777–1780, 2006.
17. Schurig, D., J. J. Mock, B. J. Justice, S. A. Cummer, J. B. Pendry, A. F. Starr, and D. R. Smith, "Metamaterial electromagnetic cloak at microwave frequencies," *Science*, Vol. 314, No. 5801, 977–980, 2006.
18. Li, J. and J. B. Pendry, "Hiding under the carpet: A new strategy for cloaking," *Physical Review Letters*, Vol. 101, 203901, 2008.
19. Cheng, X., H. Chen, B. I. Wu, and J. A. Kong, "Cloak for bianisotropic and moving media," *Progress In Electromagnetics Research*, Vol. 89, 199–212, 2009.
20. Cheng, Q., W. X. Jiang, and T. J. Cui, "Investigations of the electromagnetic properties of three-dimensional arbitrarily-shaped cloaks," *Progress In Electromagnetics Research*, Vol. 94, 105–117, 2009.
21. Cheng, X., H. Chen, X.-M. Zhang, B. Zhang, and B. I. Wu, "Cloaking a perfectly conducting sphere with rotationally uniaxial nihility media in monostatic radar system," *Progress In Electromagnetics Research*, Vol. 100, 285–298, 2010.
22. Lai, Y., J. Ng, H. Y. Chen, D. Han, J. Xiao, Z. Q. Zhang, and C. T. Chan, "Illusion optics: The optical transformation of an object into another object," *Physical Review Letters*, Vol. 102, 253902, 2009.

23. Duan, Z. Y., B. I. Wu, S. Xi, H. S. Chen, and M. Chen, "Research process in reversed cherenkov radiation in double-negative metamaterials," *Progress In Electromagnetics Research*, Vol. 90, 75–87, 2009.
24. Silveirinha, M. and N. Engheta, "Tunneling of electromagnetic energy through subwavelength channels and bends using  $\epsilon$ -near-zero materials," *Physical Review Letters*, Vol. 97, 157403, 2006.
25. Silveirinha, M. and N. Engheta, "Design of matched zero-index metamaterials using nonmagnetic inclusions in epsilon-near-zero media," *Physical Review B*, Vol. 75, 075119, 2007.
26. Silveirinha, M. G. and N. Engheta, "Theory of supercoupling, squeezing wave energy, and field confinement in narrow channels and tight bends using  $\epsilon$  near-zero metamaterials," *Physical Review B*, Vol. 76, 245109, 2007.
27. Alu, A. and N. Engheta, "Dielectric sensing in  $\epsilon$ -near-zero narrow waveguide channels," *Physical Review B*, Vol. 78, 045102, 2008.
28. Alu, A., M. G. Silveirinha, and N. Engheta, "Transmission-line analysis of  $\epsilon$ -near-zero-filled narrow channels," *Physical Review E*, Vol. 78, 016604, 2008.
29. Edwards, B., A. Alu, M. G. Silveirinha, and N. Engheta, "Reflectionless sharp bends and corners in waveguides using epsilon-near-zero effects," *Journal of Applied Physics*, Vol. 105, No. 4, 044905, 2009.
30. Liu, R., Q. Cheng, T. Hand, J. J. Mock, T. J. Cui, S. A. Cummer, and D. R. Smith, "Experimental demonstration of electromagnetic tunneling through an epsilon-near-zero metamaterial at microwave frequencies," *Physical Review Letters*, Vol. 100, 023903, 2008.
31. Edwards, B., A. Alu, M. E. Young, M. Silveirinha, and N. Engheta, "Experimental verification of epsilon-near-zero metamaterial coupling and energy squeezing using a microwave waveguide," *Physical Review Letters*, Vol. 100, 033903, 2008.
32. Halterman, K. and S. Feng, "Resonant transmission of electromagnetic fields through subwavelength zero- $\epsilon$  slits," *Physical Review A*, Vol. 78, 021805, 2008.
33. Ziolkowski, R. W., "Propagation in and scattering from a matched metamaterial having a zero index of refraction," *Physical Review E*, Vol. 70, 046608, 2004.
34. Enoch, S., G. Tayeb, P. Sabouroux, N. Guerin, and P. Vincent, "A metamaterial for directive emission," *Physical Review Letters*, Vol. 89, 213902, 2002.
35. Alu, A., M. G. Silveirinha, A. Salandrino, and N. Engheta,

- “Epsilon-near-zero metamaterials and electromagnetic sources: Tailoring the radiation phase pattern,” *Physical Review B*, Vol. 75, 155410, 2007.
36. Hao, J., W. Yan, and M. Qiu, “Super-reflection and cloaking based on zero index metamaterial,” *Applied Physics Letters*, Vol. 96, No. 10, 101109, 2010.
  37. Jin, Y. and S. He, “Enhancing and suppressing radiation with some permeability-near-zero structures,” *Optics Express*, Vol. 18, No. 16, 16587–16593, 2010.
  38. Nguyen, V. C., L. Chen, and K. Halterman, “Total transmission and total reflection by zero index metamaterials with defects,” *Physical Review Letters*, Vol. 105, 233908, 2010.
  39. Xu, Y. and H. Chen, “Total reflection and transmission by epsilon-near-zero metamaterials with defects,” *Applied Physics Letters*, Vol. 98, No. 11, 113501, 2011.
  40. Wang, L. G., Z. G. Wang, J. X. Zhang, and S. Y. Zhu, “Realization of Dirac point with double cones in optics,” *Optics Letters*, Vol. 34, No. 10, 1510–1512, 2009.
  41. Novoselov, K. S., A. K. Geim, S. V. Morozov, D. Jiang, Y. Zhang, S. V. Dubonos, I. V. Grigorieva, and A. A. Firsov, “Electric field effect in atomically thin carbon films,” *Science*, Vol. 306, No. 5696, 666–669, 2004.
  42. Novoselov, K. S., A. K. Geim, S. V. Morozov, D. Jiang, M. I. Katsnelson, I. V. Grigorieva, S. V. Dubonos, and A. A. Firsov, “Two-dimensional gas of massless dirac fermions in grapheme,” *Nature*, Vol. 438, 197–200, 2005.
  43. Zhang, Y., Y. W. Tan, H. L. Stormer, and P. Kim, “Experimental observation of the quantum hall effect and Berry’s phase in grapheme,” *Nature*, Vol. 438, 201–204, 2005.
  44. Katsnelson, M. I., K. S. Novoselov, and A. K. Geim, “Chiral tunnelling and the Klein paradox in graphene,” *Nature Physics*, Vol. 2, 620–625, 2006.
  45. Morozov, S. V., K. S. Novoselov, M. I. Katsnelson, F. Schedin, L. A. Ponomarenko, D. Jiang, and A. K. Geim, “Strong suppression of weak localization in graphene,” *Physical Review Letters*, Vol. 97, 016801, 2006.
  46. Neto, A. H. C., F. Guinea, N. M. R. Peres, K. S. Novoselov, and A. K. Geim, “The electronic properties of grapheme,” *Reviews of Modern Physics*, Vol. 81, 109–162, 2009.
  47. Geim, A. K. and A. H. MacDonald, “Graphene: Exploring carbon flatland,” *Physics Today*, Vol. 60, No. 8, 35–41, 2007.

48. Geim, A. K. and K. S. Novoselov, "The rise of graphene," *Nature Materials*, Vol. 6, 183–191, 2007.
49. Huang, X., Y. Lai, Z. H. Hang, H. Zheng, and C. T. Chan, "Dirac cones induced by accidental degeneracy in photonic crystals and zero-refractive-index materials," *Nature Materials*, Vol. 10, 582–586, 2011.
50. Liu, F., X. Huang, and C. T. Chan, "Dirac cones at  $k = 0$  in acoustic crystals and zero refractive index acoustic materials," *Applied Physics Letters*, Vol. 100, No. 7, 071911, 2012.
51. Liu, F., Y. Lai, X. Huang, and C. T. Chan, "Dirac cones at  $k = 0$  in phononic crystals," *Physical Review B*, Vol. 84, 224113, 2011.
52. Plihal, M. and A. A. Maradudin, "Photonic band structure of a two-dimensional system: The triangular lattice," *Physical Review B*, Vol. 44, 8565, 1991.
53. Haldane, F. D. M. and S. Raghu, "Possible realization of directional optical waveguides in photonic crystals with broken time-reversal symmetry," *Physical Review Letters*, Vol. 100, 013904, 2008.
54. Raghu, S. and F. D. M. Haldane, "Analogues of quantum-hall-effect edge states in photonic crystals," *Physical Review A*, Vol. 78, 033834, 2008.
55. Ochiai, T. and M. Onoda, "Photonic analog of graphene model and its extension: Dirac cone, symmetry, and edge states," *Physical Review B*, Vol. 80, 155103, 2009.
56. Ochiai, T., "Topological properties of bulk and edge states in honeycomb lattice photonic crystals: The case of TE polarization," *Journal of Physics: Condensed Matter*, Vol. 22, No. 22, 225502, 2010.
57. Sepkhanov, R. A., J. Nilsson, and C. W. J. Beenakker, "Proposed method for detection of the pseudospin —  $1/2$  Berry phase in a photonic crystal with a Dirac spectrum," *Physical Review B*, Vol. 78, 045122, 2008.
58. Mei, J., Y. Wu, C. T. Chan, and Z. Q. Zhang, "First-principles study of Dirac and Dirac-like cones in phononic and photonic crystals," *Physical Review B*, Vol. 86, 035141, 2012.
59. Sepkhanov, R. A., Y. B. Bazaliy, and C. W. J. Beenakker, "Extremal transmission at the Dirac point of a photonic band structure," *Physical Review A*, Vol. 75, 063813, 2007.
60. Diem, M., T. Koschny, and C. M. Soukoulis, "Transmission in the vicinity of the Dirac point in hexagonal photonic crystals," *Physica B*, Vol. 405, 2990–2995, 2010.

61. Zhang, X., "Observing Zitterbewegung for photons near the Dirac point of a two-dimensional photonic crystal," *Physical Review Letters*, Vol. 100, 113903, 2008.
62. Zhang, X. and Z. Liu, "Extremal transmission and beating effect of acoustic waves in two-dimensional sonic crystals," *Physical Review Letters*, Vol. 101, 264303, 2008.
63. Wang, L. G., Z. G. Wang, and S. Y. Zhu, "Zitterbewegung of optical pulses near the dirac point inside a negative-zero-positive index metamaterial," *EPL*, Vol. 86, 47008, 2009.
64. Sakoda, K., "Dirac cone in two- and three-dimensional metamaterials," *Optics Express*, Vol. 20, No. 4, 3898–3917, 2012.
65. Sakoda, K. and H. Zhou, "Role of structural electromagnetic resonances in a steerable left-handed antenna," *Optics Express*, Vol. 18, No. 26, 27371–27386, 2010.
66. Sakoda, K. and H. Zhou, "Analytical study of two-dimensional degenerate metamaterial antennas," *Optics Express*, Vol. 19, No. 15, 13899–13921, 2011.
67. Sakoda, K., "Double Dirac cones in triangular-lattice metamaterials," *Optics Express*, Vol. 20, No. 9, 9925–9939, 2012.
68. Inui, T., Y. Tanabe, and Y. Onodera, *Group Theory and Its Applications in Physics*, Springer, Berlin, 1990.
69. Wu, Y., J. Li, Z. Q. Zhang, and C. T. Chan, "Effective medium theory for magnetodielectric composites: Beyond the long-wavelength limit," *Physical Review B*, Vol. 74, 085111, 2006.
70. Sakoda, K., *Optical Properties of Photonic Crystals*, 2nd Edition, Springer-Verlag, Berlin, 2004.
71. Li, J. and C. T. Chan, "Double-negative acoustic metamaterial," *Physical Review E*, Vol. 70, 055602, 2004.
72. Wu, Y. and Z. Q. Zhang, "Dispersion relations and their symmetry properties of electromagnetic and elastic metamaterials in two dimensions," *Physical Review B*, Vol. 79, 195111, 2009.